Available online at www.sciencedirect.com
ScienceDirect
Trans. Nonferrous Met. Soc. China 34(2024) 194−202
Transactions of Nonferrous Metals Society of China
www.tnmsc.cn

Collaborative optimization of microstructure, phase composition and room-temperature fracture toughness of Nb−Si based alloys using Ti, Zr and Hf elements

Qi WANG[1], Tian-yu ZHAO[1], Rui-run CHEN[1], Xiao-wei WANG[1], Qin XU[1,2], Shu WANG[1], Heng-zhi FU[1]

1. National Key Laboratory for Precision Hot Processing of Metals, School of Materials Science and Engineering, Harbin Institute of Technology, Harbin 150001, China;
2. School of Mechanic and Electrical Engineering, Henan University of Technology, Zhengzhou 450001, China

Received 6 June 2022; accepted 30 June 2023

Abstract: The Nb−16Si−*x*Ti−*y*Zr−*z*Hf (*x*=18, 22; *y*=0, 4; *z*=0, 4; at.%) alloys were prepared by arc melting to investigate the influence of elements Ti, Zr and Hf additions on the phase constitution, microstructure, fracture toughness and crack propagation behavior. The results show that the single addition of 4 at.% Zr promotes the eutectoid reaction of $(Nb,X)_3Si$ phase to Nb solid solution (Nbss)/γ-$(Nb,X)_5Si_3$ eutectic, and simultaneous addition of Ti, Zr and Hf further promotes the eutectoid reaction. The crack trends to propagate in $(Nb,X)_3Si$ phase, and the crack deflects when the crack meets Nbss. The fine Nbss/γ-$(Nb,X)_5Si_3$ eutectic and Nbss/γ-$(Nb,X)_5Si_3$ lamellar structures can induce the crack bridging and branching, and hinder the crack growth. Nb−16Si−22Ti−4Zr−4Hf alloy with the highest content of alloying elements exhibits the highest room-temperature fracture toughness (11.62 MPa·m$^{1/2}$), which is 87.7% higher than that of the Nb−16Si−18Ti alloy. The performance improvement is mainly attributed to the presence of lamellar eutectic structure.

Key words: Nb−Si alloy; alloying; fracture toughness; crack propagation

1 Introduction

Nb−Si based alloys with relatively low densities, good elevated-temperature strengths and high melting points are regarded as the promising super-temperature composite material, used in the next generation turbine blade at temperature as high as 1200 °C, which are supposed to replace nickel base single crystal superalloy for elevated temperature structural applications in future turbofan engine [1−3]. Nb_5Si_3 phase with the high melting point of 2484 °C provides elevated-temperature mechanical properties and oxidation resistance, and the Nb solid solution (Nbss) provides the toughness in Nb−Si based alloys [4−6]. However, the insufficient fracture toughness and ductility restrict the industrial application of Nb−Si based alloys.

There are usually two ways to improve fracture toughness of Nb−Si based alloys, including alloying and processing technologies [7−10]. Alloying is an effective means to improve the toughness of Nb−Si based alloys, which has attracted a great deal of attention [5−8]. Large number of alloying elements have been introduced to Nb−Si based alloys, including Ti [5−10], V [11,12], Zr [4,13,14], Hf [15,16], B [17,18], C [19] and so on. However, some alloying elements are detrimental to the room-temperature fracture toughness, including Cr [20,21], Al [21,22], Mo [15,19] and so on. The addition of Ti in Nb−Si

Corresponding author: Rui-run CHEN, Tel/Fax: +86-451-86412394, E-mail: ruirunchen@hit.edu.cn;
Tian-yu ZHAO, E-mail: 21B309027@stu.hit.edu.cn
DOI: 10.1016/S1003-6326(23)66391-5

based alloys can reduce the element P−N barrier energy of Nbss phase, which increases the toughness of Nbss phase [9,10]. Therefore, newly developed Nb−Si based alloys usually contain a greater content of Ti element, and develop into the ternary Nb−Si−Ti based alloys. 4−8 at.% Hf element is commonly added in Nb−Si based alloys for improving fracture toughness and oxidation resistance [15,16]. Recent studies have shown that 4 at.% Zr can significantly improve the room-temperature fracture toughness of Nb−Si based alloys [4,13]. Hf, Zr and Ti are IV-B elements, and the same group elements added to metal alloys usually have similar effects on microstructure and mechanical properties. However, there is less study on the effect of simultaneous addition of Hf, Zr and Ti elements on mechanical properties and microstructure of Nb−Si based alloys, which arouses our interest. This study evaluated the common effect of adding Hf, Zr and Ti elements on microstructural evolution and fracture toughness of Nb−Si based alloys. A particular attention is paid on the crack propagation performance after fracture toughness testing.

2 Experimental

Button ingots of Nb−Si based elevated-temperature alloys were prepared by arc melting, and the raw materials used in this experiment are Nb (99.95 at.%), Si (99.9 at.%), Zr (99.9 at.%), Ti (99.95 at.%) and Hf (99.9 at.%). All button ingots in this study were melted in a water-cooled copper crucible, by non-consumable tungsten electrode, under purified Ar gas. And all button ingots were melted four times for homogenous distribution of alloying elements. X-ray diffraction (XRD, under 40 kV and scanning speed of 8 (°)/min, using the Cu K_α radiation) was used to identify the constituent phases in the investigated alloys. Microstructure of the investigated alloys was observed by scanning electron microscopy (SEM, Quanta 200FEG) equipped with backscattered electron mode (BSE), and the energy disperse spectroscopy based on SEM was performed to measure the chemical composition of specimens. Due to the contrast of phases under SEM is different, Image J software was used to calculate the area fraction of phases. The final area fraction of each phase was calculated by taking three images of different locations and calculating the average.

The single-edge notched room-temperature fracture toughness was measured on an electronic universal mechanical testing machine (Instron 5569) and the crosshead speed was 0.2 mm/min. Electrode discharge machine was performed to cut 2.0 mm deep slit notches in fracture toughness testing specimen for fracture toughness testing. At least three specimens were tested and the average value was employed for room temperature fracture toughness of the investigated alloys. Crack profile data were based on similar fracture toughness testing specimens that were tested under similar testing condition. In the stress state, microcrack occurred at the intersection of prefabricated crack and the surface of specimen. The propagation of crack under stress state was analyzed by the microcrack [23]. Microcrack is much less extensive in the sample than that at the free surface of the specimen.

3 Results and discussion

3.1 Phase constitution and microstructure

The addition of Hf, Zr and Ti can significantly improve the room-temperature fracture toughness of Nb−Si based alloys, and 4−8 at.% Hf [15,17], 4 at.% Zr [13,17] and 18−22 at.% Ti [8−10] are usually added in Nb−Si based alloys. Therefore, the 4 at.% Hf, 4 at.% Zr, 18 Ti at.% or 22 Ti at.% were added in Nb−16Si based alloys in this study. The nominal compositions of investigated alloys are given in Table 1 (all chemical compositions are given in at.% in this work). Figure 1 shows the XRD patterns of investigated alloys. The Nb−16Si−18Ti, Nb−16Si−22Ti, Nb−16Si−18Ti−4Hf and Nb−16Si−22Ti−4Hf alloys have the same phase composition, including $(Nb,X)_3Si$ and Nbss phases ("X" represents the elements substituting for Nb in the lattices), and they have similar characteristic peaks, which indicates that the 4 at.% Hf addition has little influence on the phase composition for Nb−16Si−18Ti and Nb−16Si−22Ti alloys. The $(Nb,X)_3Si$, Nbss and γ-$(Nb,X)_5Si_3$ phases are detected in Nb−16Si−18Ti−Zr, Nb−16Si−18Ti−4Zr−4Hf, Nb−16Si−22Ti−4Zr and Nb−16Si−22Ti−4Zr−4Hf alloys, which indicates that the addition of 4 at.% Zr contributes to the formation of γ-$(Nb,X)_5Si_3$ phase.

Table 1 Nominal compositions of Nb−Si-based alloys

Alloy	Nominal composition/at.%				
	Nb	Si	Ti	Zr	Hf
Nb−16Si−18Ti	66	16	18	−	−
Nb−16Si−18Ti−4Zr	62	16	18	4	−
Nb−16Si−18Ti−4Hf	62	16	18	−	4
Nb−16Si−18Ti−4Zr−4Hf	58	16	18	4	4
Nb−16Si−22Ti	62	16	22	−	−
Nb−16Si−22Ti−4Zr	58	16	22	4	−
Nb−16Si−22Ti−4Hf	58	16	22	−	4
Nb−16Si−22Ti−4Zr−4Hf	54	16	22	4	4

Figure 2 shows BSE-SEM images of Nb−16Si−18Ti, Nb−16Si−18Ti−4Zr, Nb−16Si−18Ti−4Hf and Nb−16Si−18Ti−4Zr−4Hf alloys. Combined with XRD results, the microstructures of Nb−16Si−18Ti and Nb−16Si−18Ti−4Hf alloys consist of primary Nbss phase, $(Nb,X)_3Si$ phase and fine Nbss/γ-$(Nb,X)_3Si$ eutectic, as shown in Figs. 2(a, c). The microstructures of Nb−16Si−18Ti−4Zr and Nb−16Si−18Ti−4Zr−4Hf alloys consist of primary Nbss phase, $(Nb,X)_3Si$ phase and fine Nbss/γ-$(Nb,X)_5Si_3$ eutectic. Table 2 lists the area fractions of Nbss phase, $(Nb,X)_3Si$ phases, and Nbss/γ-$(Nb,X)_5Si_3$ eutectic in investigated alloys. The result shows that the addition of 4 at.% Hf has little influence on the microstructure and phase composition, as shown in Figs. 2(a, c). However, the addition of 4 at.% Zr contributes to the formation of fine Nbss/γ-$(Nb,X)_5Si_3$ eutectic, as shown in Figs. 2(b, d).

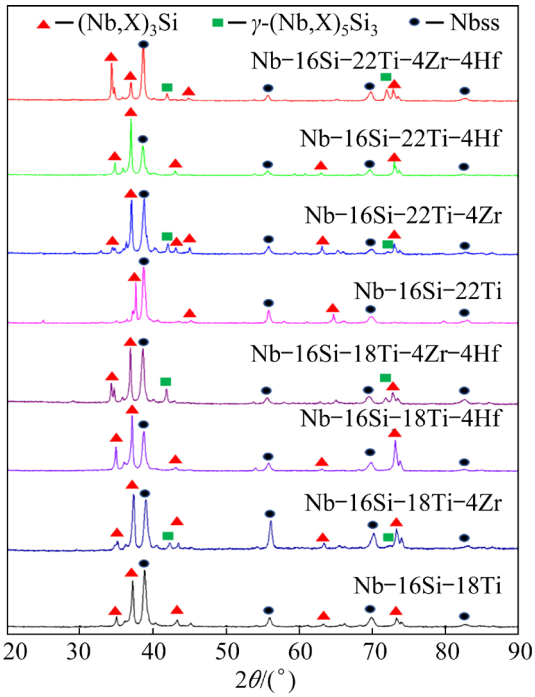

Fig. 1 XRD patterns of investigated alloys

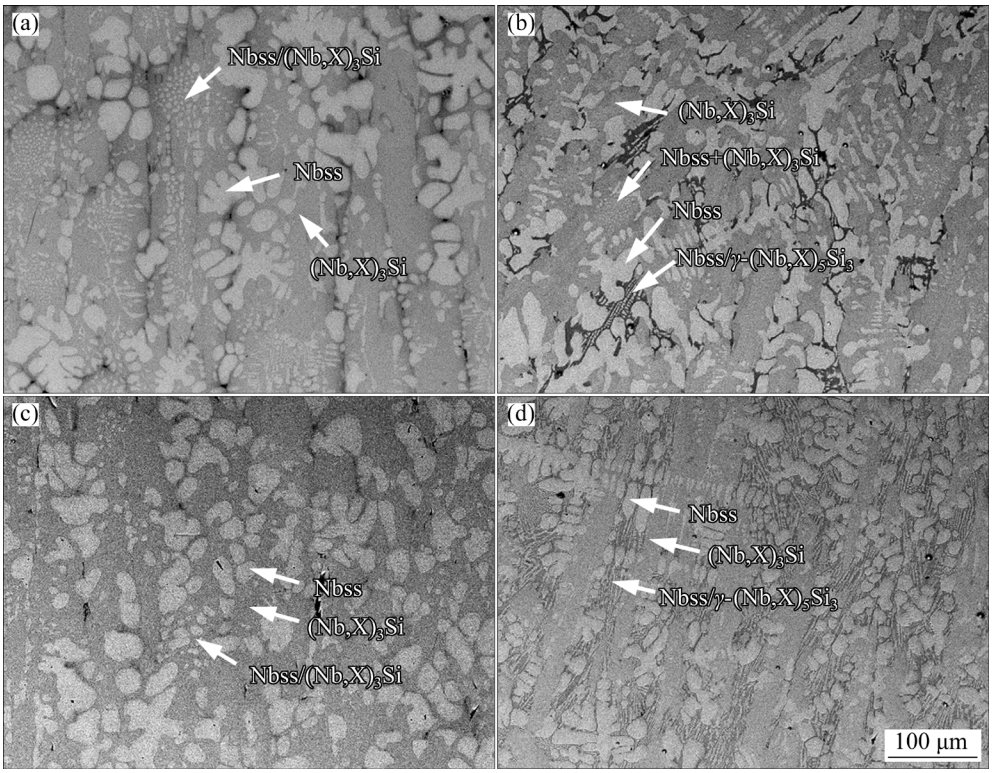

Fig. 2 BSE-SEM images of Nb−16Si−18Ti (a), Nb−16Si−18Ti−4Zr (b), Nb−16Si−18Ti−4Hf (c) and Nb−16Si−18Ti−4Zr−4Hf (d) alloys

Table 2 Area fractions of Nbss and $(Nb,X)_3Si$ phase, and Nbss/γ-$(Nb,X)_5Si_3$ eutectic in investigated alloys (%)

Alloy	Nbss	$(Nb,X)_3Si$ phase	Nbss/γ-$(Nb,X)_5Si_3$ eutectic
Nb−16Si−18Ti	42	58	−
Nb−16Si−18Ti−4Zr	38	54	8
Nb−16Si−18Ti−4Hf	40	60	−
Nb−16Si−18Ti−4Zr−4Hf	36	44	20
Nb−16Si−22Ti	40	60	−
Nb−16Si−22Ti−4Zr	35	53	12
Nb−16Si−22Ti−4Hf	43	57	−
Nb−16Si−22Ti−4Zr−4Hf	31	43	26

Moreover, the area fraction of Nbss/γ-$(Nb,X)_5Si_3$ eutectic in the Nb−16Si−18Ti−4Zr−4Hf alloy significantly increases compared with Nb−16Si−18Ti−4Zr alloy, which indicates that simultaneous addition of Zr and Hf elements contributes to the formation of fine Nbss/γ-$(Nb,X)_5Si_3$ eutectic.

Figures 3 shows BSE-SEM images of Nb−16Si−22Ti, Nb−16Si−22Ti−4Zr, Nb−16Si−22Ti−4Hf and Nb−16Si−22Ti−4Zr−4Hf alloys. Combined with the XRD results, the microstructure and phase composition in Nb−16Si−22Ti and Nb−16Si−22Ti−4Hf alloys are similar to those of Nb−16Si−18Ti and Nb−16Si−18Ti−4Hf alloys. However, the area fractions of fine Nbss/γ-$(Nb,X)_5Si_3$ eutectic in Nb−16Si−22Ti−4Zr and Nb−16Si−22Ti−4Zr−4Hf alloys significantly increase compared with those of Nb−16Si−18Ti−4Zr and Nb−16Si−18Ti−4Zr−4Hf alloys. The fine Nbss/γ-$(Nb,X)_5Si_3$ eutectic is surrounded by Nbss, which indicates that Nbss substitutes $(Nb,X)_3Si$ phase in the matrix. This result suggests that Zr addition contributes to the eutectoid reaction of $(Nb,X)_3Si$ phase to Nbss/γ-$(Nb,X)_5Si_3$ eutectic.

Previous studies have reported that the additions of Hf, Zr or Ti can contribute to the formation of $(Nb,X)_5Si_3$ phase [13−16]. In this study, the microstructure and phase composition are not significantly different in Nb−16Si−18Ti, Nb−16Si−18Ti−4Hf, Nb−16Si−22Ti and Nb−22Si−22Ti−4Hf alloys. For alloys containing Zr element (Nb−16Si−18Ti−4Zr, Nb−16Si−18Ti−4Zr−4Hf, Nb−16Si−22Ti−4Zr and Nb−16Si−22Ti−4Zr−4Hf), the area fraction of Nbss/γ-$(Nb,X)_5Si_3$ eutectic increases with the content of Hf, Zr and Ti element in alloys, as shown in Table 2. This result suggests that the Hf, Zr and Ti elements contribute to the formation of γ-$(Nb,X)_5Si_3$ phase. However, for alloys which only contain Hf element (Nb−16Si−18Ti−4Hf and Nb−22Si−22Ti−4Hf), $(Nb,X)_5Si_3$ phase does not exist in the microstructure, as shown in Figs. 2 and 3. Compared with alloys containing

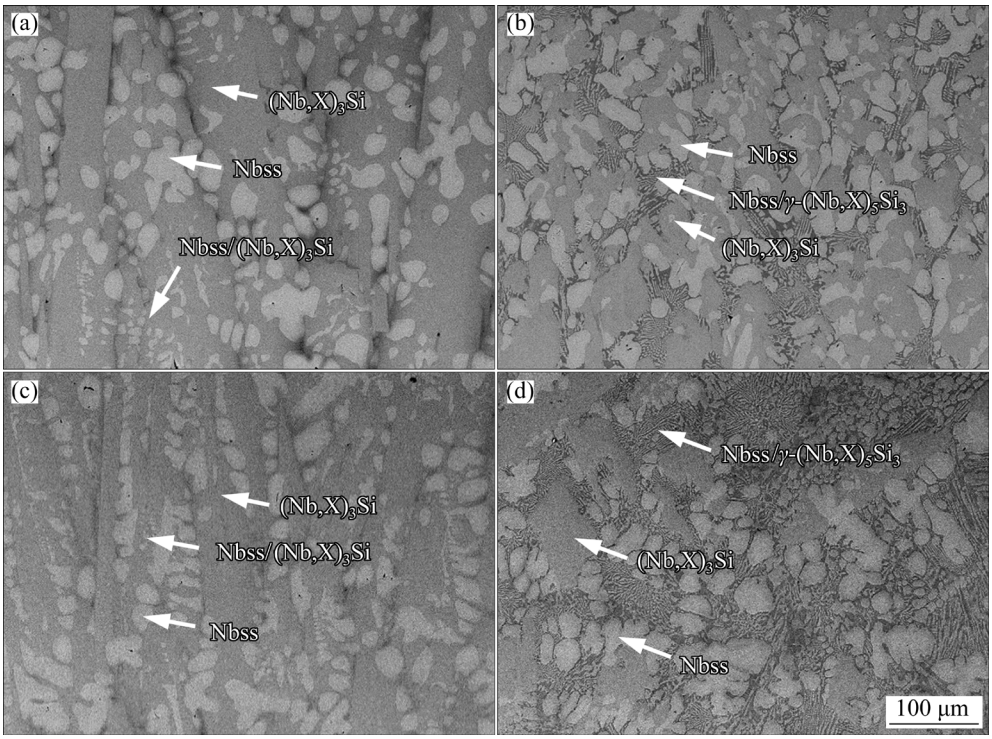

Fig. 3 BSE-SEM images of Nb−16Si−22Ti (a), Nb−16Si−22Ti−4Zr (b), Nb−16Si−22Ti−4Hf (c) and Nb−16Si−22Ti−4Zr−4Hf (d) alloys

Zr element, it can be inferred that the stabilization effect of Zr element on $(Nb,X)_5Si_3$ phase is stronger than Hf and Ti elements.

3.2 Fracture toughness

Figure 4 shows the average room-temperature fracture toughness (K_Q) of investigated alloys. The K_Q value of Nb−16Si−18Ti alloy is 6.19 MPa·m$^{1/2}$. The addition of 4 at.% Zr in Nb−16Si−18Ti alloy results in K_Q value increasing to 10.32 MPa·m$^{1/2}$, improved by 66.7%. The K_Q value of Nb−16Si−18T−4Hf alloy is 6.84 MPa·m$^{1/2}$, which is similar to that of Nb−16Si−18Ti alloy. The simultaneous addition of 4 at.% Zr and 4 at.% Hf in Nb−16Si−18Ti alloy results in the K_Q value increasing to 10.92 MPa·m$^{1/2}$, which is similar to that of Nb−16Si−18Ti−4Zr alloy. The K_Q value of 22 at.% Ti-contained alloys is slightly higher compared with 18 at.% Ti-contained alloys. Nb−16Si−22Ti−4Zr−4Hf alloy with the highest content of alloying elements exhibits the highest room-temperature fracture toughness (11.62 MPa·m$^{1/2}$), which is 87.7% higher than that of Nb−16Si−18Ti alloy. To sum up, the Zr-contained alloys exhibit a higher room-temperature fracture toughness.

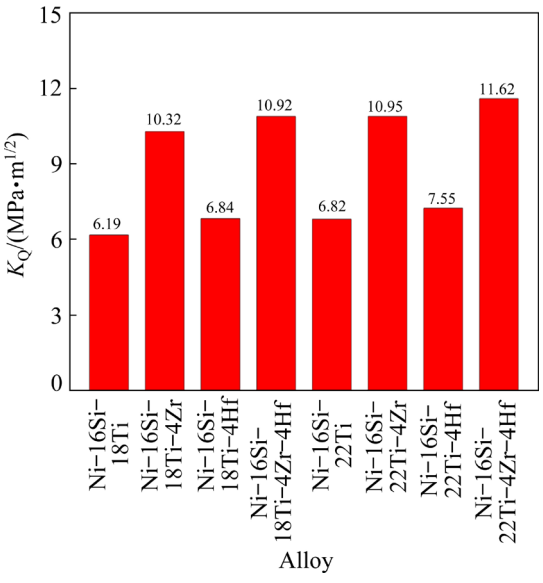

Fig. 4 Average room-temperature fracture toughness (K_Q) of investigated alloys

3.3 Crack propagation behavior

Figures 5 and 6 show BSE-SEM micro-structures of the crack propagation path after fracture toughness test, and the crack propagation mechanisms are studied in this study. The Nb−16Si−18Ti, Nb−16Si−18Ti−4Hf, Nb−16Si−22Ti and Nb−16Si−22Ti−4Hf alloys have the similar microstructure and phase composition, and they show the similar crack propagation behavior after fracture toughness test, as shown in Figs. 5(a, e) and 6(a, e). There is a clear tendency for the crack to propagate in the $(Nb,X)_3Si$ matrix, or along the interface between silicide phase and Nbss, and the crack usually deflects when the crack meets Nbss. The crack bridging and branching usually occur when the crack path is perpendicular to Nbss. It can be observed that the second cracking occurs in the Nb_3Si phase when the crack propagation encounters Nbss.

The Nb−16Si−18Ti−4Zr, Nb−16Si−18Ti−4Zr−4Hf, Nb−16Si−22Ti−4Zr, and Nb−16Si−22Ti−4Zr−4Hf alloys contain convoluted Nbss/γ-$(Nb,X)_5Si_3$ eutectic, as shown in Figs. 5(c, g) and 6(c, g). The special microstructure of regular lamellar structures of Nbss/γ-$(Nb,X)_5Si_3$ eutectic is found in Nb−16Si−18Ti−4Zr−4Hf alloy, as shown Fig. 5(h), and there is a clear tendency for the crack propagation parallel to the regular lamellar structures of Nbss/γ-$(Nb,X)_5Si_3$ eutectic. The similar result has been found in TiAl alloys that the regular lamellar structures could contribute to crack propagation, which is harmful to the room-temperature fracture toughness [24,25]. However, when the angle between the propagation direction of crack and lamellar direction is large, the crack branching and deflection occur, which improves the crack propagation resistance. Compared with the lamellar structures of Nbss/γ-$(Nb,X)_5Si_3$ eutectic, the crack is easier to bypass globular Nbss. Therefore, the special microstructure of regular lamellar structures of Nbss/γ-$(Nb,X)_5Si_3$ eutectic can improve the fracture toughness of Nb−Si alloy.

Figure 7 shows the schematic diagram of crack growth of investigated alloys based on the room-temperature fracture toughness testing results. Figures 7(a, b, c) show the schematic diagrams of the crack propagating in the silicide phase, perpendicular to Nbss, and along the regular Nbss/γ-$(Nb,X)_5Si_3$ lamellar structures, respectively. The crack branching and crack bridging are therefore the mechanisms of energy dissipation that contributes to the toughness of Nb−Si based alloys. The crack bridging is found in region of Nbss/γ-$(Nb,X)_5Si_3$ eutectic, but the regular Nbss/γ-$(Nb,X)_5Si_3$ lamellar structures contribute to crack growth, which suggests that the microstructure of

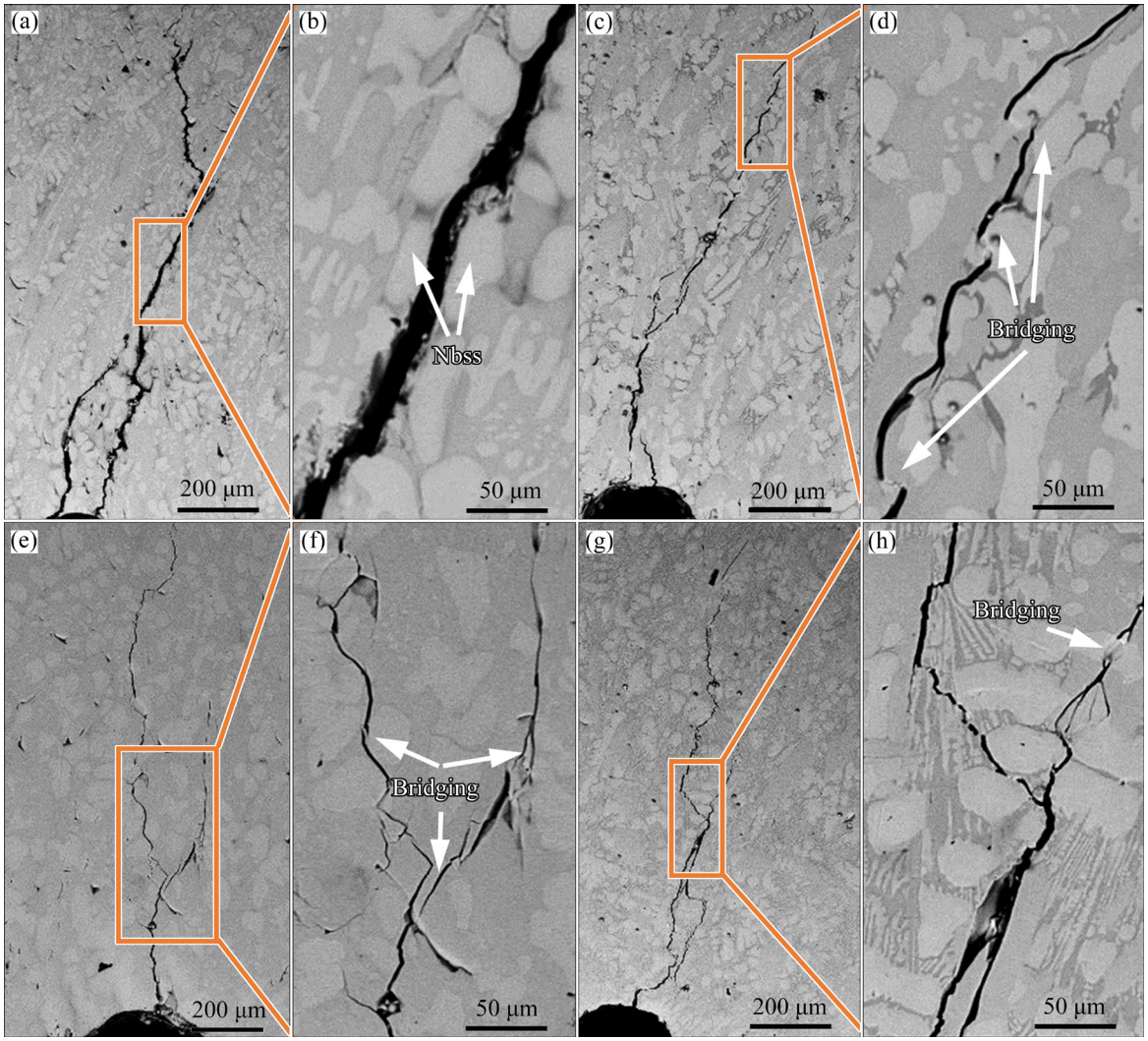

Fig. 5 Crack propagation path of Nb−16Si−18Ti (a, b), Nb−16Si−18Ti−4Zr (c, d), Nb−16Si−18Ti−4Hf (e, f), and Nb−16Si−18Ti−4Zr−4Hf (g, h) alloys after room-temperature fracture tests

high fracture toughness Nb−Si based alloys has the following characteristics: (1) The matrix of Nb−Si based alloy contains the fine Nbss/γ-$(Nb,X)_5Si_3$ eutectic; (2) There is a certain amount of Nbss/γ-$(Nb,X)_5Si_3$ lamellar structures in the region of Nbss/γ-$(Nb,X)_5Si_3$ eutectic; (3) Nbss has a high continuity, since Nbss can hinder the crack growth. Figure 6(g) shows that the crack grows mainly through the lamellar Nbss/γ-$(Nb,X)_5Si_3$ eutectic structure. The continuous Nbss phase in the lamellar eutectic structure causes more deflections and bridging, and also generates secondary cracks. According to above mechanisms, these consume stress greatly, leading to the best room-temperature fracture toughness of Nb−16Si−18Ti−4Zr−4Hf alloy.

Previous studies have shown that the addition of Hf, Zr and Ti have a solution strengthening on Nbss [11−13], which improves the room-temperature fracture toughness of Nbss, and the addition of the same group elements to metal alloys usually have similar effect on mechanical properties [4,13,15,16]. In this study, the addition of 22 at.% Ti slightly improves the fracture toughness of the alloy compared with the 18 at.% Ti-contained Nb−Si alloy. The addition of 4 at.% Hf has little influence on the room-temperature fracture toughness, because the addition of 4 at.% Hf has little influence on the microstructure. The addition of 4 at.% Zr significantly improves the room-temperature fracture toughness of investigated alloys, which can be attributed to the following reasons. (1) The addition of Zr contributes to the formation of fine Nbss/γ-$(Nb,X)_5Si_3$ eutectic and

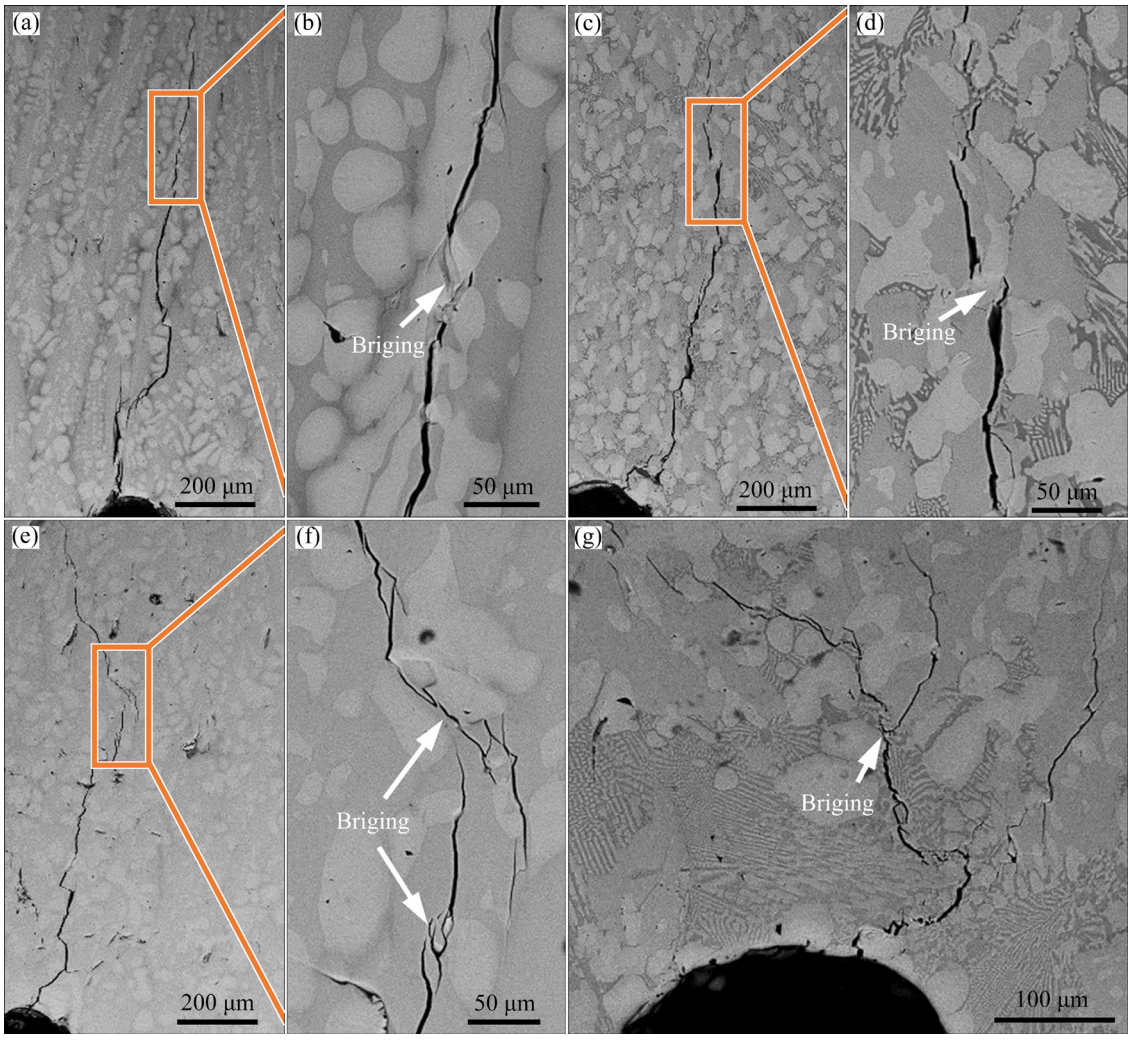

Fig. 6 Crack propagation path of Nb−16Si−22Ti (a, b), Nb−16Si−22Ti−4Zr (c, d), Nb−16Si−22Ti−4Hf (e, f) and Nb−16Si−18Ti−4Zr−4Hf (g) alloys after room-temperature fracture tests

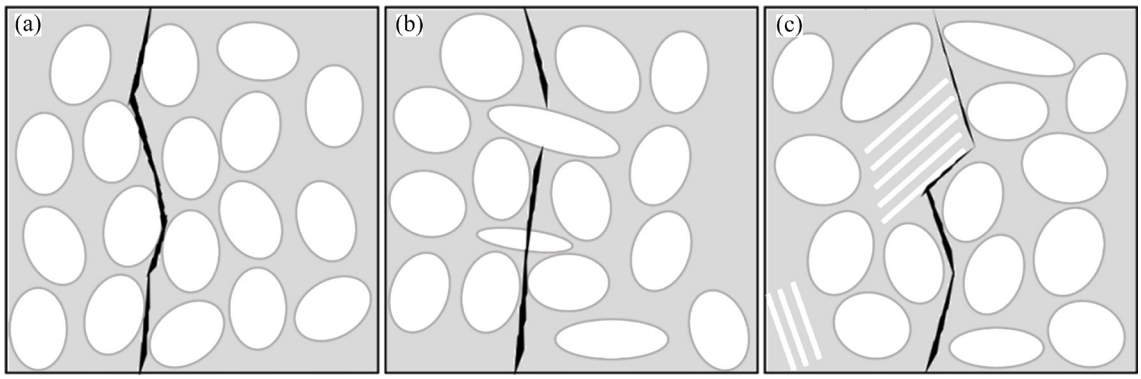

Fig. 7 Schematic diagrams of crack growth of Nb−Si based alloys: (a) In silicide phase; (b) Perpendicular to Nbss; (c) Along regular Nbss/γ-$(Nb,X)_5Si_3$ lamellar structures

Nbss/γ-$(Nb,X)_5Si_3$ lamellar structures, which hinders the crack growth. (2) The addition of Zr in Nb−Si based alloys has a solid solution strengthening effect on Nbss, and thus improves fracture toughness [4,13]. The Zr-contained Nb−Si alloy exhibits a high fracture toughness compared with Hf-contained Nb−Si alloy, and Zr element exhibits low cost and low density compared with Hf element, which indicates that Zr is a promising alloying element for Nb−Si alloy.

4 Conclusions

(1) The addition of 4 at.% Hf or 22 at.% Ti has a little influence on the microstructure and phase composition, and the addition of 4 at.% Zr contributes to the eutectic reaction of $(Nb,X)_3Si$ phase to Nbss/γ-$(Nb,X)_5Si_3$ eutectic.

(2) There is a clear tendency for the crack to propagate in the $(Nb,X)_3Si$ matrix, or along the interface between the silicide phase and Nbss, and the crack deflects when the crack meets Nbss.

(3) The fine Nbss/γ-$(Nb,X)_5Si_3$ eutectic and Nbss/γ-$(Nb,X)_5Si_3$ lamellar structures can induce the crack bridging and branching, and hinder the crack growth.

(4) Nb−16Si−22Ti−4Zr−4Hf alloy with the highest contents of alloying elements exhibits the highest room-temperature fracture toughness (K_Q=11.62 MPa·m$^{1/2}$), which is 87.7% higher than that of Nb−16Si−18Ti alloy. Compared with Nb−16Si−18Ti and Nb−16Si−22Ti alloys, the K_Q values of Nb−16Si−18Ti−4Zr (10.92 MPa·m$^{1/2}$) and Nb−16Si−22Ti−4Zr (10.95 MPa·m$^{1/2}$) are much improved. The improvement of properties is mainly derived from the existence of Zr element, which contributes to the formation of fine Nbss/γ-$(Nb,X)_5Si_3$ eutectic and plays a solid solution strengthening on Nbss. Therefore, Zr is a promising alloying element for Nb−Si alloy.

CRediT authorship contribution statement

Qi WANG: Resources, Funding acquisition, Writing − Review & editing; **Tian-yu ZHAO:** Methodology, Formal analysis, Writing − Original draft; **Rui-run CHEN:** Conceptualization, Validation, Supervision, Project administration; **Xiao-wei WANG:** Software; **Qin XU:** Investigation; **Shu WANG:** Data curation; **Heng-zhi FU:** Visualization.

Declaration of competing interest

The authors declare that they have no known competing financial interests or personal relationships that could have appeared to influence the work reported in this paper.

Acknowledgments

The authors gratefully acknowledge support from the National Natural Science Foundation of China (No. 51825401), the Foundation of National Key Laboratory for Precision Hot Processing of Metals, China (No. JCKYS2021603C001), and the Natural Science Foundation of Heilongjiang Province, China (No. LH2020E032).

References

[1] YE Cheng-tong, JIA Li-na, JIN Zu-heng, WANG Yu, ZHANG Hu. Directional solidification of hypereutectic Nb−Si−Ti alloy: Influence of drawing velocity change on microstructures [J]. Journal of Alloys and Compounds, 2020, 844: 156123.

[2] YOON J K, KIM G H. Accelerated oxidation behavior of Nb−Si_2 coating grown on Nb substrate at 600−900 °C [J]. Corrosion Science, 2018, 141: 97−108.

[3] WAN Bei-bei, ZHANG Hua-rui, GAO Ming, BAI Peng, ZHANG Hu. High-temperature wettability and interactions between Hf-containing NbSi-based alloys and Y_2O_3 ceramics with various microstructures [J]. Materials & Design, 2018, 138: 103−110.

[4] SANKAR M, PHANIKUMAR G, SINGH V, SATYA PRASAD V V. Effect of Zr additions on microstructure evolution and phase formation of Nb−Si based ultrahigh temperature alloys [J]. Intermetallics, 2018, 101: 123−132.

[5] KONG Bin, JIA Li-na, ZHANG Hu, SHA Jiang-bo, SHI Song-xin, GUAN Kai. Microstructure, mechanical properties and fracture behavior of Nb with minor Si addition [J]. International Journal of Refractory Metals and Hard Materials, 2016, 58: 84−91.

[6] BEWLAY B P, JACKSON M R, ZHAO Ji-cheng. A review of very-high-temperature Nb-suicide-based composites [J]. Metallurgical and Materials Transaction A, 2003, 34(10): 2043−2052.

[7] TSAKIROPOULOS P. Alloys for application at ultra-high temperatures: Nb−silicide in situ composites: Challenges, breakthroughs and opportunities [J]. Progress in Materials Science, 2022, 123: 100714.

[8] WANG Fu-xin, LUO Liang-shun, MENG Xian-yu, XU Yan-jin, WANG Liang, SU Yan-qing, GUO Jing-jie, FU Heng-zhi. Morphological evolution of primary β-Nb_5Si_3 phase in Nb−Mo−Si alloys [J]. Journal of Alloys and Compounds, 2018, 741: 51−58.

[9] ZELENITSAS K, TSAKIROPOULOS P. Study of the role of Al and Cr addition in the microstructure of Nb−Ti−Si in situ composites [J]. Intermetallics, 2005, 13: 1079−1095.

[10] GUO Yue-ling, JIA Li-na, KONG Bin, ZHANG Hua-rui, ZHANG Hu. Simultaneous improvement in fracture toughness and oxidation resistance of Nb−Si based alloys by vanadium addition [J]. Materials Science and Engineering A, 2017, 701: 149−157.

[11] KANG Yong-wang, QU Shi-yu, Song Jin-xia, HUANG Qiang, HAN Ya-fang. Microstructure and mechanical properties of Nb−Ti−Si−Al−Hf−xCr−yV multi-element in situ composite [J]. Materials Science and Engineering A, 2012, 534: 323−328.

[12] KIM W Y, YEO I D, RA T Y, Cho G S, KIM M S. Effect of V addition on microstructure and mechanical property in the

Nb−Si alloy system [J]. Journal of Alloys and Compounds, 2004, 364: 186−192.
[13] TIAN Yu-xin, GUO Jian-ting, SHENG Li-yuan, CHENG Guang-ming, ZHOU Lan-zhang, HE Lian-long, YE Heng-qiang. Microstructures and mechanical properties of cast Nb−Ti−Si−Zr alloys [J]. Intermetallics, 2008, 16: 807−812.
[14] SALA K, MITRA R. Effect of Zr or Ga addition and annealing on microstructural evolution, deformation and fracture behavior of Nb−19Si−5Mo−20Ti based hypereutectic alloy [J]. Metallurgical and Materials Transactions A, 2022, 53: 1717−1737.
[15] KIM J H, TABARU T, SAKAMOTO M, HANADA S. Mechanical properties and fracture behavior of an Nbss/Nb_5Si_3 in-situ composite modified by Mo and Hf alloying [J]. Materials Science and Engineering A, 2004, 372: 137−144.
[16] ZHAO Ji-cheng, BEWLAY B P, JACKSON M R. Determination of Nb−Hf−Si phase equilibria [J]. Intermetallics, 2001, 9: 681−689.
[17] ZHANG Song, GUO Xi-ping. Microstructural characteristics of Nb−Si based ultrahigh temperature alloys with B and Hf additions [J]. Intermetallics, 2015, 64: 51−58.
[18] SUN Zhi-ping, GUO Xi-ping, TIAN Xiao-dong, ZHOU Liang. Effects of B and Si on the fracture toughness of the Nb−Si alloys [J]. Intermetallics, 2014, 54: 143−147.
[19] SHA Jiang-bo, HIRAI H, TABARU T, KITAHARA A, UENO H, HANADA S. Effect of carbon on microstructure and high-temperature strength of Nb−Mo−Ti−Si in situ composites prepared by arc-melting and directional solidification [J]. Materials Science and Engineering A. 2003, 343: 282−289.
[20] ZHANG Song-ming, SHI Xing-rui, SHA Jiang-bo. Microstructural evolution and mechanical properties of as-cast and directionally-solidified Nb−15Si−22Ti−2Al−2Hf−2V−(2,14)Cr alloys at room and high temperatures [J]. Intermetallics, 2015, 56: 15−23.
[21] CHAN K S. A computational approach to designing ductile Nb−Ti−Cr−Al solid-solution alloys [J]. Metallurgical and Materials Transactions A, 2001, 32: 2475−2487.
[22] SHAO Gao. Thermodynamic assessment of the Nb−Si−Al system [J]. Intermetallics, 2004, 12: 655−664.
[23] BARBI N, DIOLOGENT F, GOODALL R, MORTENSEN A. Fracture toughness of TiAl alloys: A comparison of two gamma-alpha 2 structures [C]//Structural Aluminides for Elevated Temperatures. TMS, 2008: 89−96.
[24] WANG Qi, CHEN Rui-run, GONG Xue, GUO Jing-jie, SU Yan-qing, DING Hong-sheng, FU Heng-zhi. Microstructure, mechanical properties and crack propagation behavior in high-Nb TiAl alloys by directional solidification [J]. Metallurgical and Materials Transactions A, 2018, 49: 4555−4564.
[25] WANG Qi, CHEN Rui-run, YANG Yao-hua, GUO Jing-jie, SU Yan-qing, DING Hong-sheng, FU Heng-zhi. Effects of grain size and precipitated phases on mechanical properties in TiAl gradient alloys [J]. Materials Science and Engineering A, 2018, 731: 634−641.

Ti、Zr 和 Hf 元素协同优化 Nb−Si 基合金显微组织、相组成和室温断裂韧性

王 琪[1]，赵天宇[1]，陈瑞润[1]，王晓伟[1]，徐 琴[1,2]，王 墅[1]，傅恒志[1]

1. 哈尔滨工业大学 材料科学与工程学院 金属精密热加工国家重点实验室，哈尔滨 150001；
2. 河南工业大学 机电工程学院，郑州 450001

摘 要：采用真空电弧熔炼制备 Nb−16Si−*x*Ti−*y*Zr−*z*Hf (*x*=18, 22; *y*=0, 4; *z*=0, 4；摩尔分数，%)合金并研究 Ti、Zr 与 Hf 元素对 Nb−Si 合金物相组成、显微组织、断裂韧性以及裂纹扩展行为的影响。结果表明：单独添加 4% Zr 元素能促进$(Nb,X)_3Si$ 向 Nb 固溶体(Nbss)/γ-$(Nb,X)_5Si_3$ 共析反应的发生；同时添加 Ti、Zr、Hf 元素能进一步促进共析反应的发生。裂纹倾向于在$(Nb,X)_3Si$ 中扩展，当裂纹途径 Nb 固溶体时会发生偏转。细密的 Nbss/γ-$(Nb,X)_5Si_3$ 共晶组织以及层状 Nbss/γ-$(Nb,X)_5Si_3$ 共晶组织可以使裂纹产生桥接与分支，阻碍裂纹的扩展。Nb−16Si−22Ti−4Zr−4Hf 的合金化元素含量最高，因此，其室温断裂韧性最好(11.62 MPa·$m^{1/2}$)，相较于 Nb−16Si−18Ti 提高 87.7%，性能的提升主要归因于存在层状共晶组织。

关键词：Nb−Si 合金；合金化；断裂韧性；裂纹扩展

(Edited by Bing YANG)